Journal of
Materials Chemistry A

ROYAL SOCIETY
OF CHEMISTRY

PAPER

View Article Online
View Journal | View Issue

Cite this: *J. Mater. Chem. A*, 2021, **9**, 16405

Two-dimensional crystalline covalent triazine frameworks *via* dual modulator control for efficient photocatalytic oxidation of sulfides†

Xuepeng Wang,‡[a] Siquan Zhang,‡[a] Xia Li,[c] Zhen Zhan,[a] Bien Tan,[a] Xianjun Lang [c] and Shangbin Jin *[ab]

Received 10th May 2021
Accepted 19th June 2021

DOI: 10.1039/d1ta03951b

rsc.li/materials-a

Two-dimensional crystalline covalent triazine frameworks (2D-CTFs) are emerging 2D materials with the characteristics of fully annulated conjugated structures and aromatic nitrogen-rich skeletons. Due to the difficulty in the control of the polymerization dynamics, the preparation of crystalline 2D-CTFs is still a daunting challenge compared to that of other organic framework materials. Herein, we report the construction of crystalline 2D-CTFs using dual modulator control, in which aniline and a co-solvent are used as dual modulators for a dynamic covalent linkage formation and non-covalent self-assembly process, respectively. The strategy successfully leads to crystalline CTFs from different functional building blocks. The crystalline CTFs could be further regulated *via* peripheral functionalization, which dramatically boosted the photocatalytic activity for oxidation of sulfides into sulfoxides, and excellent conversion rates and selectivity for a wide range of sulfides with various functional groups were achieved after functionalization with methoxyl groups. This work gives new insights into the design and synthesis of crystalline CTFs for photocatalytic applications.

1. Introduction

Two-dimensional (2D) organic crystalline materials, such as 2D covalent organic frameworks (2D-COFs), have attracted enormous research attention due to their 2D layered and tailorable structures.[1–13] 2D-CTFs, a subtype of 2D-COFs, are built from triazine and other aromatic rings, and possess highly stable and annulated porous structures, making them ideal candidates for gas adsorption,[14–17] photocatalysis,[18–21] energy storage,[22–26] and heterogeneous catalysis.[27–29] It has been considered that the crystalline stacking structures and ordered pore structures are key advantages of COFs for their functional applications, which could provide ordered molecular diffusion or charge transport pathways.[30–32] However, the crystallinity of the state-of-the-art 2D-CTFs remains incomparable with that of 2D-COFs with more reversible linkages, such as boronate-linked or imine-linked 2D-COFs. 2D-CTFs with higher crystallinity are in demand for advancing their applications.

Crystalline organic frameworks are mainly regulated by the dynamic covalent chemistry *via* reversible covalent linkages and self-assembly processes *via* non-covalent interactions.[33] According to dynamic covalent chemistry, the reversibility in the linkage or framework is the essential prerequisite to attain high crystallinity. Nevertheless, 2D-CTFs have usually suffered from poor reversibility, mainly because of the low reversibility of intermediate bonds in the trimerization or condensation reactions, as well as the fully conjugated stable frameworks. Although, a variety of strategies have been reported to increase their crystallinity, such as monomer concentration control in the polycondensation reaction,[34,35] interfacial trimerization reaction,[36,37] ionothermal trimerization at high temperatures,[9,38] and microwave-assisted trimerization or other multi-step transformation methods,[39,40] it is still a challenge to modulate their crystallinity effectively under mild conditions. Recently, dynamic control of imine linkage using a modulator has been found very effective to obtain highly crystalline imine-linked organic frameworks.[41–44] However, the implementation of such a strategy in 2D-CTFs has been critically challenging due to the low reversibility and the strict reaction conditions in the conventional methods. On the other hand, the noncovalent interlayer control should be an important part for the generation of crystalline 2D-CTFs, because it may affect the crystal growth in the self-assembly process *via* π–π stacking. However, it has been paid very little attention and how the crystallinity of 2D-CTFs is affected by the non-covalent approach is unclear. If we could merge the dynamic covalent chemistry with the non-

---

[a] *School of Chemistry and Chemical Engineering, Huazhong University of Science and Technology, Luoyu Road 1037, Wuhan, 430074, China*

[b] *School of Chemical Engineering and Technology, Xi'an Jiaotong University, Xianning West Road, Xi'an, Shaanxi, 710049, China. E-mail: shangbin@xjtu.edu.cn*

[c] *Sauvage Center for Molecular Sciences, College of Chemistry and Molecular Sciences, Wuhan University, Wuhan 430072, China*

† Electronic supplementary information (ESI) available. See DOI: 10.1039/d1ta03951b

‡ These authors contributed equally to this work.

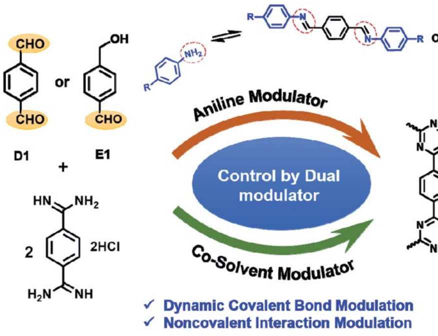

Scheme 1 Representative schematic view of the dual modulator control for the synthesis of crystalline 2D-CTFs.

covalent self-assembly process, the assessment of higher crystalline 2D-CTFs may be possible.

Herein, we report the synthesis of crystalline 2D-CTFs *via* a dual modulator control, that is, through dynamic control of covalent linkage using an aniline modulator and noncovalent self-assembly regulation using a co-solvent modulator (Scheme 1). The modulation of the reaction dynamics in 2D-CTFs was realized by using an aniline modulator in the polycondensation reaction, due to the presence of an intermediate imine-bond before the cyclization. And the noncovalent modulation was accomplished by introducing an aromatic co-solvent as a second modulator to modulate the crystallization process in CTFs. Assisted by the two modulators, we successfully achieved 2D-CTFs with greatly enhanced crystallinity. With the establishment of this strategy, the crystalline CTFs with variable structures were shown to achieve high photocatalytic performance in the oxidation of sulfides, and exhibited excellent yield and selectivity after installing electron donating units as the peripheral side groups in the CTFs' pore walls.

2. Experimental section

2.1 Materials

p-Phthalaldehyde, cesium carbonate (Cs_2CO_3), *p*-phthalaldehyde, 4-(hydroxymethyl)benzaldehyde, 2,5-dimethoxyterephthalaldehyde, terephthalamidine, aniline, *p*-toluidine, 2,4,6-trimethylaniline, 4-bromoaniline, toluene, mesitylene, *n*-hexadecane, *o*-dichlorobenzene (*o*-DCB), benzene-1,4-dicarbonitrile, lithium bis(trimethylsilyl)amide, *N*,*N*-dimethylformamide (DMF), tetrahydrofuran (THF) and dimethyl sulfoxide (DMSO) were purchased from Aladdin Reagent (Shanghai) Co., Ltd.

2.2 Synthesis of CTF materials

The reaction monomers and an aniline modulator were dispersed in dimethyl sulfoxide (DMSO) and a co-solvent modulator, and then the mixtures were heated for reaction to yield the corresponding crystalline CTFs (see the ESI† for the detailed process). The crystalline CTFs obtained from *p*-phthalaldehyde and 4-(hydroxymethyl)-benzaldehyde are labelled CTF-HUST-D1 and CTF-HUST-E1, respectively. The products obtained without adding aniline modulators under the same conditions were named CTF-HUST-d1 and CTF-HUST-e1, respectively.

The general synthesis procedure was as follows: a mixture of aldehyde monomer (0.5 mmol), terephthalamidine (1.0 mmol), Cs_2CO_3 (2.2 mmol), aniline derivatives (according to actual experiments required) and DMSO or other mixed solvents (10 mL) were added into a flask. Then the reaction was heated at 100 °C for 24 h, 120 °C for 24 h and 160 °C for 48 h. After cooling to room temperature, the mixture was washed with DMF and water. The detailed process can be found in the ESI.†

3. Results and discussion

3.1 Aniline and co-solvent dual modulator control

We at first studied the influence of the aniline modulators on the crystallinity. According to the reaction mechanism, the monofunctional aniline modulators could react with the bisaldehyde monomers at the outset. Therefore, the aniline modulators in the polycondensation reaction of CTFs could inhibit the direct reaction of aldehyde-based monomers with amidine, and hence may effectively regulate the nucleation and crystal growth processes of CTFs. We evaluated the anilines which are incorporated with various substitutional groups, including aniline, *p*-toluidine, 2,4,6-trimethylaniline, and 4-bromoaniline. As shown in Fig. 1a, *p*-toluidine incorporated with an electron donating group ($-CH_3$) is proven to be the most effective modulator among the series, and the peak intensity at 7.4° in the PXRD of the CTF sharply increased (blue curve). Aniline without any substitutional group also works well to enhance the crystallinity (Fig. 1a, red curve). In contrast, when 4-bromoaniline incorporated with an electron withdrawing group (–Br) was used, the crystallinity was not improved (Fig. 1a, purple curve). Although 2,4,6-trimethylaniline is more electron donating, the crystallinity of the CTF remains almost unchanged (Fig. 1a, green curve), which may be related to large steric hindrance in the structure. These observations indicate that the reactivities

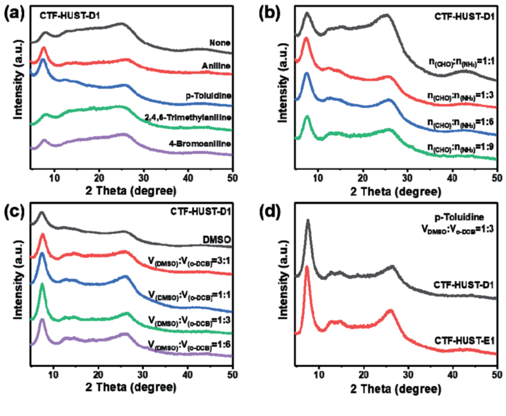

Fig. 1 Experimental PXRD patterns of the crystalline CTFs: (a) influence of different aniline modulators, (b) influence of the amount of *p*-toluidine ($n_{(NH_2)}$ represents the molar amounts of aniline modulators), (c) the ratio of mixed solvent of DMSO and *o*-dichlorobenzene (*o*-DCB), (d) the crystallinity of CTF-HUST-D1 and CTF-HUST-E1 under optimal conditions.

of amino groups in these aniline modulators are crucial to the dynamic control process and thus have influence on the crystallinity. This increased crystallinity in the CTFs was indicated by the increased ordinate peak intensity and the shrunken background of the PXRD. Due to the competitive reactions, excess amounts of aniline modulators are needed. We noted that when the amounts of anilines are three times those of aldehyde monomers, the optimal result is accomplished in terms of yield and crystallinity (Fig. 1b, red curve). Too excessive amounts, however, reduced the yields of CTFs (Fig. 1b, green curve). The CTF-HUST-E1 obtained from the 4-(hydroxymethyl)-benzaldehyde monomer (with a single aldehyde group) also possesses excellent crystallinity when using the same synthesis conditions (Fig. 1d and S1b–d†). However, when 1,4-benzenedimethanol (without the aldehyde group) was used as the monomer under the same conditions, the corresponding CTF cannot be obtained. This phenomenon implies that the aldehyde group is indispensable in this strategy.

After investigation of the aniline modulators for the dynamic covalent process, we next explored the influence of the non-covalent process on the crystallinity. Solvents play an important role in accessing crystalline COFs.[45–47] The use of the solvent effect is also an important way to access noncovalent self-assembly systems.[48,49] To our surprise, the influence of the solvent effect has been rarely explored in CTFs. In previous studies of CTFs synthesized by the polycondensation reaction, only a single solvent has been used, where DMSO works as the sole reaction medium as well as the oxidant.[34,35,50,51] DMSO is a good solvent for monomers and oligomers because of its high polarity. We assumed that the combination of DMSO solvent with non-polar solvents, particularly aromatic solvents, may be able to control the self-assembly process in the crystallization of 2D-CTFs. Various aromatic or nonpolar organic solvents, including toluene, mesitylene, *o*-dichlorobenzene (*o*-DCB), or *n*-hexadecane, were hence adopted as the co-solvent. We found that mesitylene, *o*-DCB and *n*-hexadecane are beneficial for the generation of higher crystallinity. Among them, the combination of DMSO with *o*-DCB gives the most positive result (Fig. S1a†). We further revealed that the solvent ratio is critical to the crystallinity, and the highest crystallinity of CTF-HUST-D1 is achieved when the volume ratio of DMSO/*o*-DCB is 1 : 3 (Fig. 1c, green curve). The reason for the enhanced crystallinity may be due to that the solvents of low polarities are conducive to the assembly of the monomers or oligomers (nucleus) in the crystallization,[52] and thereby are capable of modulating the crystal growth in a much ordered manner.

As shown in Fig. 2a, after adding *p*-toluidine and a co-solvent as dual modulators, the crystallinities of CTF-HUST-D1 and CTF-HUST-E1 were significantly enhanced, which is clearly evidenced by the prominently enhanced peak intensity at 7.4° and their narrowed half-width. By comparing the full width at half maxima (FWHM) of the peak at 7.4° in PXRD patterns with those of the previously reported CTF-HUST-HC1 (FWHM: 1.91) and CTF-HUST-C1 (FWHM: 1.67) measured under the same conditions (Fig. 2b and Table S1†), the FWHM of the peaks in CTF-HUST-D1 (FWHM: 1.52) and CTF-HUST-E1 (FWHM: 1.45) were obviously narrowed. Furthermore, the intensities of the peak at 7.4° in PXRD were increased by nearly two times. These results indicate that the present strategy is more effective than the previous methods.[34,35]

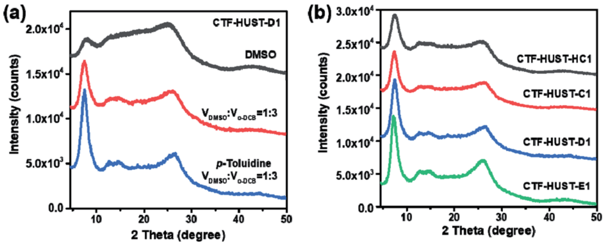

Fig. 2 (a) Experimental powder X-ray diffraction patterns of the CTFs under different conditions. (b) Comparison of the PXRD of CTFs synthesized by the present method with that of the CTFs from previous methods.

3.2 Structural characterization

The resulting crystalline 2D-CTFs were unambiguously characterized. Fourier-transformed infrared (FT-IR) spectra were recorded to characterize the CTFs' structures. The characteristic peaks at 1518 cm^{-1} (–C=N–) and 1352 cm^{-1} (–C–N=) belonging to the triazine moiety in CTF-HUST-D1 and CTF-HUST-E1 are in line with previous work (Fig. 3a).[50] The characteristic chemical shift of the triazine carbon atom is at 170 ppm and the assignment of the other carbon atoms as shown in the solid-state ^{13}C NMR spectra can also confirm the desired structures (Fig. 3b). Elemental analysis shows that the carbon, nitrogen and oxygen contents of CTFs are close to the theoretical values (Table S2†). X-ray photoelectron spectroscopy (XPS) revealed the bonding type of each element in CTFs. As shown in Fig. 3c and d, the high-resolution C 1s and N 1s surveys of CTF-HUST-D1 and CTF-HUST-E1 display peaks at 287.3 eV and 399.2 eV, which are assigned to C=N–C of the triazine moiety.[51] The peaks were fitted with a single peak,

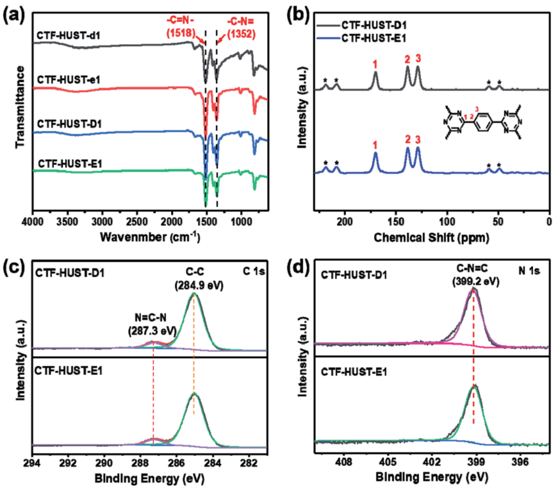

Fig. 3 FT-IR spectra (a), solid-state ^{13}CNMR spectra (b), high-resolution XPS C 1s and N 1s spectra (c and d) for CTF-HUST-D1 and CTF-HUST-E1.

indicating the lesser defective structures formed in this strategy.

The morphologies of CTFs were investigated by scanning electron microscopy (SEM). Compared with CTF-HUST-d1 and CTF-HUST-e1 that are synthesized only using DMSO solvent in the absence of aniline modulators, CTF-HUST-D1 and CTF-HUST-E1 synthesized from the mixed solvent system (DMSO and *o*-DCB) comprise much larger particle sizes (Fig. S2a–e†). This implies that the crystal growth is more favored when the competitive reaction occurs with aniline modulators. By nitrogen sorption–desorption tests, the Brunauer–Emmett–Teller (BET) surface areas for CTF-HUST-D1 and CTF-HUST-E1 are calculated to be 477 and 428 $m^2\ g^{-1}$, respectively. The average pore size distribution of CTF-HUST-D1 and CTF-HUST-E1 is centered at 1.2 nm (Fig. S2c and f†). As shown in Fig. S3,† the lattice fringes in high resolution-transmission electron microscopy (HR-TEM) clearly imply ordered structures in the local area in CTF-HUST-D1 and CTF-HUST-E1, which is also solid evidence for the crystalline structures. TEM-mapping demonstrated that the carbon and nitrogen elements are distributed evenly in the entire CTFs (Fig. S4†). Thermogravimetric analysis showed that CTF-HUST-D1 and CTF-HUST-E1 are thermally stable until 500 °C (Fig. S5†).

3.3 Photocatalytic oxidation of sulfides

In the previous studies, Wang and coworkers have shown that crystalline COFs are promising platforms for photocatalytic selective aerobic oxidation of organic sulfides.[12,13] With the establishment of the above strategy, we explored the photocatalytic applications of the resulting CTFs in this oxidation reaction. As shown in Table S3,† the initial test shows that CTF-HUST-D1 has an excellent selectivity, whereas only a low conversion rate (13%) was found within 30 min. We anticipated that the increase of electron-rich segments could improve the photocatalytic ability,[53,54] as it is more conducive to the generation of oxidative radical species. Hence, crystalline CTF-HUST-D2 was designed and synthesized by installing a methoxy group into the aldehyde monomer (Fig. 4a, b and S6–S10†). Indeed, CTF-HUST-D2 showed a much higher conversion rate of 55% than CTF-HUST-D1 (13%) within a short interval of 30 min. After extension of the reaction time, excellent conversion rate of sulfides and selectivity to products were successfully achieved. As shown in Table 1, the highest conversion rate up to 99% and selectivity up to 96% were obtained within 2 h. The catalytic reaction also showed a wide generality of sulfide substrates, indicating that it is an efficient photocatalyst with wide versatility.[12,13]

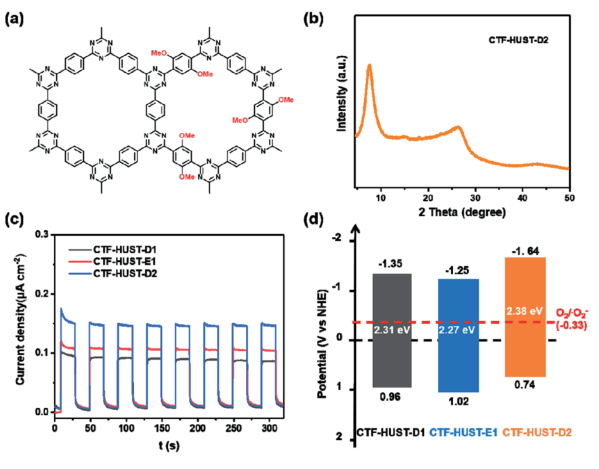

Fig. 4 (a) The structure and (b) powder X-ray diffraction patterns of CTF-HUST-D2, (c) time related transient photocurrent response, (d) energy level alignments of CTFs calculated from experimental results.

3.4 Mechanism of the photocatalytic oxidation

The photocatalysis mechanism of the CTF was next probed. Quenching experiments by employing different scavengers were

Table 1 Photocatalytic oxidation of sulfides into sulfoxides by CTF-HUST-D2[a]

Entry	Substrate	Product	*T* (h)	Conv.[b] (%)	Sel.[b] (%)
1	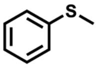	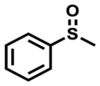	1.1	91	94
2	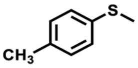	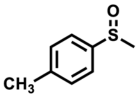	1.0	94	95
3	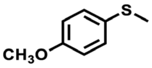	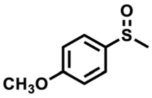	1.2	90	91
4	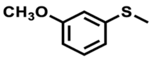	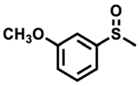	1.6	92	94
5	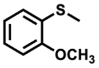	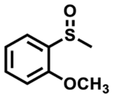	1.4	93	96
6	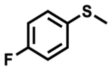	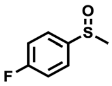	1.5	91	94
7	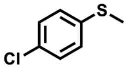	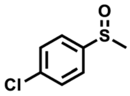	1.9	91	92
8	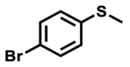	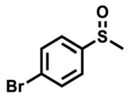	2.0	90	94
9	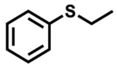	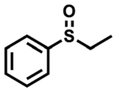	1.4	99	81
10	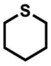	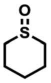	1.0	93	85

[a] Reaction conditions: sulfide (0.5 mmol), CTF photocatalyst (0.01 mmol calculated based on the repeating unit), blue LED irradiation (3 W × 4), CH_3OH (1 mL), air (1 atm). [b] Conversion and selectivity to sulfoxides, determined by GC-FID using chlorobenzene as the internal standard.

performed to identify the active species that played the major role in the catalytic process. As shown in Table S4,† when the reaction was performed in a nitrogen atmosphere, no reaction occurred, and when a superoxide radical scavenger (*p*-BQ) or electron trapper ($AgNO_3$) was added, the conversion rate and selectivity to the target product were also remarkably decreased. These results indicate that oxygen is indispensable to the catalytic reaction and the superoxide radical ($^{\bullet}O_2^-$) generated in the photocatalytic process is the essential active species for the reaction. To directly identify the existence of $^{\bullet}O_2^-$ during photocatalysis, *in situ* ESR tests were performed by employing 5,5-dimethyl-1-pyrroline *N*-oxide (DMPO) as the trapper. As shown in Fig. S11,† the characteristic ESR signals of DMPO–$^{\bullet}O_2^-$ were clearly seen for CTF-HUST-D1, CTF-HUST-E1 and CTF-HUST-D2 under visible-light irradiation. Notably, CTF-HUST-D2 displays the strongest response signal under the same conditions, which is in line with the photocatalytic results.

The electron-donating methoxy group in CTF-HUST-D2 makes its UV/visible absorption red-shifted compared to that of CTF-HUST-D1 (Fig. S12†). It not only makes the CTF exhibit a wider light response, but also makes the framework more conducive to the charge carrier photogeneration and transport (Fig. S13†). As shown in Fig. 4c, CTF-HUST-D2 has a much higher photocurrent, which indicates a higher carrier concentration.[55,56] As shown in the photoluminescence (PL) spectra (Fig. S14†), the photoluminescence intensity of CTF-HUST-D2 is obviously decreased compared to that of CTF-HUST-D1 and CTF-HUST-E1, indicating that the recombination of photogenerated carriers is restrained. The Mott–Schottky plots of CTF-HUST-D1, CTF-HUST-E1 and CTF-HUST-D2 were further investigated at frequencies of 1500 Hz, 2000 Hz and 2500 Hz (Fig. S15†). Compared to CTF-HUST-D1 and CTF-HUST-E1, the E_{LUMO} potential for CTF-HUST-D2 was upshifted to −1.64 V (Fig. 4d). The LUMO energy level of CTF-HUST-D2 is more negative than the reduction potential of $O_2/^{\bullet}O_2^-$ (−0.33 V *vs.* NHE),[57] and the photogenerated electrons of CTF-HUST-D2 could be more easily captured by the O_2 to generate $^{\bullet}O_2^-$, and then it could further react more efficiently with the sulfides to generate sulfoxides.[58] The photocatalytic performance of CTF-HUST-D2 is also superior to that of many other reported photocatalysts (Table S5†), indicating that the peripheral functionalization is very effective in enhancing the photocatalytic performance of CTFs.

4. Conclusions

In conclusion, crystalline covalent triazine framework materials (CTFs) were successfully accessed through a dual modulator control strategy, in which the aniline modulator and solvent modulator were used for the control of the covalent bond formation dynamics and self-assembly process, respectively. The strategy is more effective to synthesize crystalline CTFs than our previous methods. Moreover, by peripheral functionalization with electron-donating groups into the building blocks, the energy band structure and photoelectric properties were readily regulated so that excellent photocatalytic oxidation of aromatic sulfides into sulfoxides was realized with high conversion and selectivity. This work gives some new insights into the synthesis of crystalline CTFs, and further shows that crystalline CTFs are powerful platforms for photocatalysis applications.

Conflicts of interest

There are no conflicts to declare.

Acknowledgements

The financial support from the National Natural Science Foundation of China (Grant No. 21875078) is greatly acknowledged. We are also grateful for the support from the China Postdoctoral Science Foundation (2019M662582). The authors thank the Analysis and Testing Center of the Huazhong University of Science and Technology for their support in the characterization.

Notes and references

1 S. Y. Ding and W. Wang, *Chem. Soc. Rev.*, 2013, **42**, 548–568.

2 E. Q. Jin, M. Asada, Q. Xu, S. Dalapati, M. Addicoat, M. Brady, H. Xu, T. Nakamura, T. Heine, Q. H. Chen and D. L. Jiang, *Science*, 2017, **357**, 673–676.

3 S. Karak, K. Dey, A. Torris, A. Halder, S. Bera, F. Kanheerampockil and R. Banerjee, *J. Am. Chem. Soc.*, 2019, **141**, 7572–7581.

4 C. Lu, Y. P. Mo, Y. Hong, T. Chen, Z. Y. Yang, L. J. Wan and D. Wang, *J. Am. Chem. Soc.*, 2020, **142**, 14350–14356.

5 Z. Wang, S. Zhang, Y. Chen, Z. Zhang and S. Ma, *Chem. Soc. Rev.*, 2020, **49**, 708–735.

6 R. R. Liang, R.-H. A, S. Q. Xu, Q. Y. Qi and X. Zhao, *J. Am. Chem. Soc.*, 2020, **142**, 70–74.

7 C. Yuan, S. Fu, K. Yang, B. Hou, Y. Liu, J. Jiang and Y. Cui, *J. Am. Chem. Soc.*, 2021, **143**, 369–381.

8 P. Kuhn, M. Antonietti and A. Thomas, *Angew. Chem., Int. Ed.*, 2008, **47**, 3450–3453.

9 M. J. Bojdys, J. Jeromenok, A. Thomas and M. Antonietti, *Adv. Mater.*, 2010, **22**, 2202–2205.

10 M. Liu, L. Guo, S. Jin and B. Tan, *J. Mater. Chem. A*, 2019, **7**, 5153–5172.

11 C. Krishnaraj, H. S. Jena, K. Leus, H. M. Freeman, L. G. Benning and P. Van Der Voort, *J. Mater. Chem. A*, 2019, **7**, 13188–13196.

12 Y. Meng, Y. Luo, J. L. Shi, H. Ding, X. Lang, W. Chen, A. Zheng, J. Sun and C. Wang, *Angew. Chem., Int. Ed.*, 2020, **59**, 3624–3629.

13 K. Y. Feng, H. M. Hao, F. W. Huang, X. J. Lang and C. Wang, *Mater. Chem. Front.*, 2021, **5**, 2255–2260.

14 A. Bhunia, D. Esquivel, S. Dey, R. Fernandez-Teran, Y. Goto, S. Inagaki, P. Van Der Voort and C. Janiak, *J. Mater. Chem. A*, 2016, **4**, 13450–13457.

15 K. Park, K. Lee, H. Kim, V. Ganesan, K. Cho, S. K. Jeong and S. Yoon, *J. Mater. Chem. A*, 2017, **5**, 8576–8582.

16 G. Tuci, M. Pilaski, H. Ba, A. Rossin, L. Luconi, S. Caporali, C. Pham-Huu, R. Palkovits and G. Giambastiani, *Adv. Funct. Mater.*, 2017, **27**, 1605672.

17 Z. Yang, S. Wang, Z. Zhang, W. Guo, K. Jie, M. I. Hashim, O. S. Miljanic, D. Jiang, I. Popovs and S. Dai, *J. Mater. Chem. A*, 2019, **7**, 17277–17282.
18 S. Kuecken, A. Acharjya, L. Zhi, M. Schwarze, R. Schomaecker and A. Thomas, *Chem. Commun.*, 2017, **53**, 5854–5857.
19 X. Jiang, P. Wang and J. Zhao, *J. Mater. Chem. A*, 2015, **3**, 7750–7758.
20 C. B. Meier, R. Clowes, E. Berardo, K. E. Jelfs, M. A. Zwijnenburg, R. S. Sprick and A. I. Cooper, *Chem. Mater.*, 2019, **31**, 8830–8838.
21 J. Xie, S. A. Shevlin, Q. Ruan, S. J. A. Moniz, Y. Liu, X. Liu, Y. Li, C. C. Lau, Z. X. Guo and J. Tang, *Energy Environ. Sci.*, 2018, **11**, 1617–1624.
22 S. Hug, L. Stegbauer, H. Oh, M. Hirscher and B. V. Lotsch, *Chem. Mater.*, 2015, **27**, 8001–8010.
23 Y. Wang, J. Chen, G. Wang, Y. Li and Z. Wen, *Angew. Chem., Int. Ed.*, 2018, **57**, 13120–13124.
24 S. N. Talapaneni, T. H. Hwang, S. H. Je, O. Buyukcakir, J. W. Choi and A. Coskun, *Angew. Chem., Int. Ed.*, 2016, **55**, 3158–3163.
25 T. Zhou, Y. Zhao, J. W. Choi and A. Coskun, *Angew. Chem., Int. Ed.*, 2019, **58**, 16795–16799.
26 Y. Li, S. Zheng, X. Liu, P. Li, L. Sun, R. Yang, S. Wang, Z. S. Wu, X. Bao and W. Q. Deng, *Angew. Chem., Int. Ed.*, 2018, **57**, 7992–7996.
27 J. Roeser, K. Kailasam and A. Thomas, *ChemSusChem*, 2012, **5**, 1793–1799.
28 S. Yamaguchi, K. Kamiya, K. Hashimoto and S. Nakanishi, *Chem. Commun.*, 2017, **53**, 10437–10440.
29 H. S. Jena, C. Krishnaraj, G. Wang, K. Leus, J. Schmidt, N. Chaoui and P. Van Der Voort, *Chem. Mater.*, 2018, **30**, 4102–4111.
30 K. Iwase, T. Yoshioka, S. Nakanishi, K. Hashimoto and K. Kamiya, *Angew. Chem., Int. Ed.*, 2015, **54**, 11068–11072.
31 Y. Su, Y. Wan, H. Xu, K. I. Otake, X. Tang, L. Huang, S. Kitagawa and C. Gu, *J. Am. Chem. Soc.*, 2020, **142**, 13316–13321.
32 H. Fan, M. Peng, I. Strauss, A. Mundstock, H. Meng and J. Caro, *J. Am. Chem. Soc.*, 2020, **142**, 6872–6877.
33 T. N. Gao, T. Wang, W. Wu, Y. Liu, Q. Huo, Z. A. Qiao and S. Dai, *Adv. Mater.*, 2019, **31**, 1806254.
34 M. Liu, Q. Huang, S. Wang, Z. Li, B. Li, S. Jin and B. Tan, *Angew. Chem., Int. Ed.*, 2018, **57**, 11968–11972.
35 M. Liu, K. Jiang, X. Ding, S. Wang, C. Zhang, J. Liu, Z. Zhan, G. Cheng, B. Li, H. Chen, S. Jin and B. Tan, *Adv. Mater.*, 2019, **31**, 1807865.
36 J. Liu, W. Zan, K. Li, Y. Yang, F. Bu and Y. Xu, *J. Am. Chem. Soc.*, 2017, **139**, 11666–11669.
37 J. Liu, P. Lyu, Y. Zhang, P. Nachtigall and Y. Xu, *Adv. Mater.*, 2018, **30**, 1705401.
38 S. Y. Yu, J. Mahmood, H. J. Noh, J. M. Seo, S. M. Jung, S. H. Shin, Y. K. Im, I. Y. Jeon and J. B. Baek, *Angew. Chem., Int. Ed.*, 2018, **57**, 8438–8442.
39 S. Ren, M. J. Bojdys, R. Dawson, A. Laybourn, Y. Z. Khimyak, D. J. Adams and A. I. Cooper, *Adv. Mater.*, 2012, **24**, 2357–2361.
40 Z. Yang, H. Chen, S. Wang, W. Guo, T. Wang, X. Suo, D. E. Jiang, X. Zhu, I. Popovs and S. Dai, *J. Am. Chem. Soc.*, 2020, **142**, 6856–6860.
41 A. M. Evans, L. R. Parent, N. C. Flanders, R. P. Bisbey, E. Vitaku, M. S. Kirschner, R. D. Schaller, L. X. Chen, N. C. Gianneschi and W. R. Dichtel, *Science*, 2018, **361**, 52–57.
42 L. Ma, W. Hu, B. Mei, H. Liu, B. Yuan, J. Zang, T. Chen, L. Zou, Z. Zou, B. Yang, Y. Yu, J. Ma, Z. Jiang, K. Wen and H. Yang, *ACS Catal.*, 2020, **10**, 4534–4542.
43 C. Lu, Y. P. Mo, Y. Hong, T. Chen, Z. Y. Yang, L. J. Wan and D. Wang, *J. Am. Chem. Soc.*, 2020, **142**, 14350–14356.
44 I. Castano, A. M. Evans, H. Li, E. Vitaku, M. J. Strauss, J. L. Bredas, N. C. Gianneschi and W. R. Dichtel, *ACS Cent. Sci.*, 2019, **5**, 1892–1899.
45 A. P. Cote, A. I. Benin, N. W. Ockwig, M. O'Keeffe, A. J. Matzger and O. M. Yaghi, *Science*, 2005, **310**, 1166–11170.
46 H. M. El-Kaderi, J. R. Hunt, J. L. Mendoza-Cortés, A. P. Côté, R. E. Taylor, M. O'Keeffe and O. M. Yaghi, *Science*, 2007, 268–272.
47 Q. Fang, Z. Zhuang, S. Gu, R. B. Kaspar, J. Zheng, J. Wang, S. Qiu and Y. Yan, *Nat. Commun.*, 2014, **5**, 4503.
48 B. Zhao, R. T. Haasch and S. MacLaren, *J. Am. Chem. Soc.*, 2004, **126**, 6124–6134.
49 E. M. Pérez, L. Sańchez, G. Fernández and N. Martín, *J. Am. Chem. Soc.*, 2006, **128**, 7172–7173.
50 K. Wang, L. M. Yang, X. Wang, L. P. Guo, G. Cheng, C. Zhang, S. B. Jin, B. E. Tan and A. Cooper, *Angew. Chem., Int. Ed.*, 2017, **56**, 14149–14153.
51 S. Zhang, G. Cheng, L. Guo, N. Wang, B. Tan and S. Jin, *Angew. Chem., Int. Ed.*, 2020, **59**, 6007–6014.
52 P. Jonkheijm, P. Jonkheijm, A. P. H. J. Schenning and E. W. Meijer, *Science*, 2006, **313**, 80–83.
53 D. Veldman, S. C. J. Meskers and R. A. J. Janssen, *Adv. Funct. Mater.*, 2009, **19**, 1939–1948.
54 X. Lang, J. Zhao and X. Chen, *Angew. Chem., Int. Ed.*, 2016, **55**, 4697–4700.
55 H.-F. Ye, R. Shi, X. Yang, W.-F. Fu and Y. Chen, *Appl. Catal., B*, 2018, **233**, 70–79.
56 X. Lang, W. R. Leow, J. Zhao and X. Chen, *Chem. Sci.*, 2015, **6**, 1075–1082.
57 Y. Deng, Z. Zhang, P. Du, X. Ning, Y. Wang, D. Zhang, J. Liu, S. Zhang and X. Lu, *Angew. Chem., Int. Ed.*, 2020, **59**, 6082–6089.
58 X. Chen, K. Deng, P. Zhou and Z. Zhang, *ChemSusChem*, 2018, **11**, 2444–2452.